Impact of interface recombination on quantum efficiency of a-Si:H/c-Si solar cells based on Si wires

Alexander Gudovskikh, Dmitry Kudryashov, Artem Baranov, Alexander Uvarov, Ivan Morozov, Alina Maximova, Ekaterina Vyacheslavova, Demid Kirilenko, Alexey Mozharov*

Prof. A. S. Gudovskikh, Dr. D.A. Kudryashov, Dr. A.I. Baranov, A.V. Uvarov, Dr. I.A. Morozov, A.A. Maximova, E.A. Vyacheslavova, A, Dr. A. M. Mozharov
Alferov University, Khlopina str. 8/3, 194021, Saint-Petersburg, Russia
E-mail: gudovskikh@spbau.ru

Prof. A. S. Gudovskikh, A.A. Maximova
Saint-Petersburg Electrotechnical University "LETI", 197376
Saint-Petersburg, Russia

D. A. Kirilenko
Ioffe Institute, 194021, Saint-Petersburg, Russia

Keywords: Si wires, core shell solar cells, a-Si:H/c-Si heterojunction, interface recombination, quantum efficiency

The impact of interface states on the quantum efficiency of a-Si:H/c-Si solar cells based on Si wires is studied using simulation and experimental measurements. The key role of the Si wire geometry for sensitivity of quantum efficiency to interface states on the sidewall is demonstrated. A decrease of Si wire diameter leads to enhanced recombination at the radial interface due to full inversion of the wire. Structures based on n-Si wires with diameter of 0.5 and 1.5 μm and doping level of 2×10^{15} cm^{-3} fabricated using a combination of latex sphere lithography and cryogenic dry etching exhibit similar values of open circuit voltage (0.5 V) and strong differences for quantum efficiency spectra. For the structures based on Si wires with a radius (0.25 μm) smaller than the space-charge region (0.6 μm) losses related to interface recombination lead to decrease of the quantum efficiency in the short-wavelength region. The recombination losses may be reduced for Si wires with a radius exceeding the

This article has been accepted for publication and undergone full peer review but has not been through the copyediting, typesetting, pagination and proofreading process, which may lead to differences between this version and the Version of Record. Please cite this article as doi: 10.1002/pssa.202100339

space charge region in silicon. In case of Si with a doping level of 10^{15} - 10^{16} cm^{-3}, which is used for solar cells, the diameter of the wires should be above 1 μm.

1. Introduction

Amorphous/crystalline silicon (a-Si:H/c-Si) heterojunction solar cells feature unique advantages for silicon solar energy development such as low-temperature deposition leading to low-thermal budget, high open-circuit voltage values and less efficiency loss at higher operation temperatures.[1-5] However, photovoltaic modules can potentially be produced much cheaper than today when moving from bulk wafer cells to thin film cells on low-cost substrates such as flexible polymer. Thin film modules are made by integrating a several micrometer thin active device layer on inexpensive supporting substrates like foils of metal or polymer. Silicon is the most preferable for using as an active photovoltaic material thanks to its high abundance and non-toxicity. Through the use of a well-developed silicon production technology and a huge industrial infrastructure it is possible to rely on high productivity and low costs for such photovoltaic modules production.

Using silicon nanowires is a promising way of flexible photovoltaic modules development. [5-8] Silicon nanowires offer a variety of advantages from enhanced light trapping to quantum size effects such us band gap variation and enhanced absorption.[9-11] Recently, promising results were obtained on single-nanowire and microwire arrays silicon solar cells.[8, 12-14] However, the surface recombination is a key issue for any nano- and microwires devises, especially solar cell. The wire surface effective passivation ways were extensively studied.[15-18] An excellent passivation of the silicon surface by a-Si:H films was demonstrated by development of a-Si:H/c-Si heterojunction solar cells.[15-21] This approach was successfully approved for Si nanowires.[22]

Despite significant progress in the development, several aspects related to the a-Si:H/c-Si radial interface properties of Si wire solar cells are still required a clarification. Heterojunction silicon nanowire ensembles with different architectures have been realized using top-down wet chemical etching of bulk p-type silicon wafers and deposition of (n)a-Si:H layers. The structures with nanowires obtained on (100) substrate demonstrate a strong light trapping effect. However, recombination losses at the silicon nanowire surface drastically reduce the solar cell performance.[23] The recombination is associated with the roughness of nanowire walls at the nano-scale level.[10] Quantum efficiency and photoluminescence measurements confirm an increase of recombination losses with nanowire length, i.e nanowire sidewalls area. A strong decrease of quantum efficiency in short wavelength region was observed. However, this result is in contradiction with common behavior of a-Si:H/c-Si anisotype heterojunction solar cells. Indeed, the value of open circuit voltage is strongly affected by interface states, while quantum efficiency weakly depends on density of interface states.[24] In this paper, the impact of interface states on the performance of a-Si:H/c-Si solar cells based on Si wires is studied using simulation and experimental measurements.

2. Simulation

First, a one-dimensional model was applied to verify the effect of interfaces states on photoelectric properties of planar a-Si:H/c-Si heterojunction solar cells using AFORS-HET software. The *I-V* curves and quantum efficiency spectra (EQE) calculated using the model described in ref. [25], which takes into account the effect of interface states, are presented in **Figure 1**. The density of interface states (D_{it}) has a significant influence on open circuit voltage (V_{OC}) and fill factor, but at the same time D_{it} does not almost affect the EQE spectra and short circuit current. The last is caused by strong band bending at the a-Si:H/c-Si interface for short circuit current conditions (inset of Figure 1a). The electric field prevents the electron

diffusion toward interface and therefore reduces the surface recombination rate. However, this result contradicts the experimentally observed drop of the quantum efficiency in the short-wavelength region with an increase of the length of Si wires with a diameter of 0.2-0.3 μm, which was associated with an increase of the interface recombination.[23]

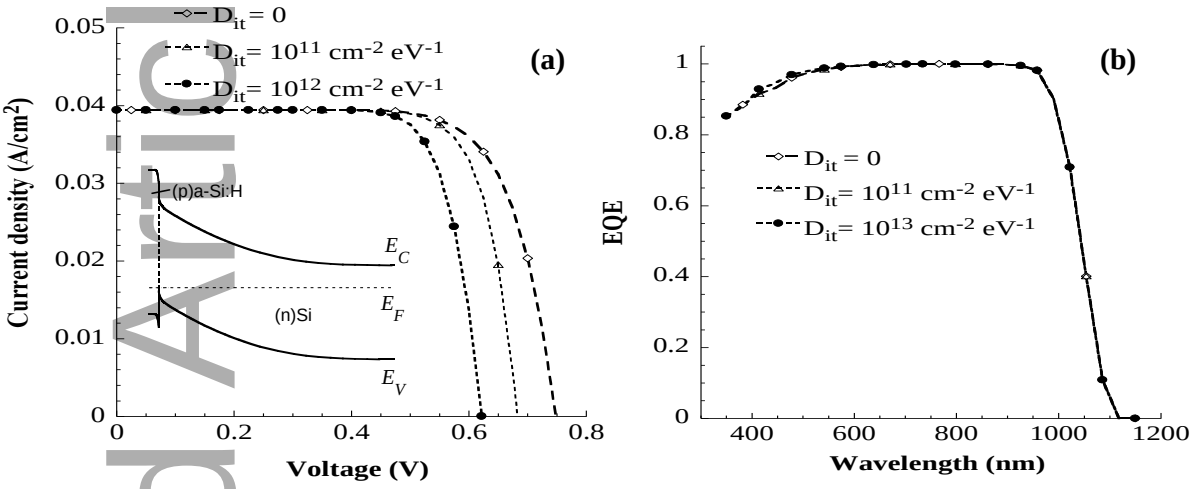

Figure 1. The *I-V* curves (a) and EQE spectra (b) calculated for planar a-Si:H/c-Si heterojunction solar cells. Band diagram is presented in the inset.

To explain the strong influence of silicon wire interface states on EQE, a three-dimensional model in a cylindrical coordinate system was developed using Silvaco TCAD software with Atlas 3D calculation module. To specify the coordinates of the semiconductor layers, a cylindrical approach to the description of the structure was used, and the coordinates of the beginning and end for the radius, angle and height for each individual layer were set. The coordinates of the computational grid were set in a similar way. The calculations were carried out using the iterative method for solving the BICGST equations (BI-Conjugate Gradient STabilized), which effectively works with more than 5000 nodes. Cylindrical crystalline n-type Si wires with a doping level of 2×10^{15} cm^{-3} and total height of 7 μm were used in the calculations of the potential profiles. The first 6 μm section from the top of a Si wire were covered by 20 nm layer of p-type doped a-Si:H, while the rest 1 μm section of Si wire at the

bottom represented the Si substrate (Figure 2a). Absorption in the n-Si substrate (300 μm, 2×10^{15} cm^{-3}) with charge carriers' lifetime of 1 ms was taken into account in calculating quantum efficiency spectra. The bottom surface of the Si substrate is covered by 20 nm of the n-type doped a-Si:H. Firstly, the simple ray tracing model with Beer–Lambert–Bouguer absorption was used. This simplification has saved calculation time.

Potential profiles calculated for Si wires with a diameter from 0.25 μm to 2 μm are shown in **Figure 2**. The calculated band diagrams along and across Si wires are also presented. For the Si wires with a diameter from 0.25 μm to 0.5 μm the space charge region is much wider (~0.6 μm for the doping level of 2×10^{15} cm^{-3}) compared to the wire radius. The Si wire is fully inverted, i.e. becomes of p-type conductivity with a high hole concentration [26], while the space charge region is located at the boundary of the inverted Si wire with n-type substrate. In this case, extremely weak band bending at the (p)a-Si:H/(n)Si radial interface is observed in the band diagram (Figure 2b).

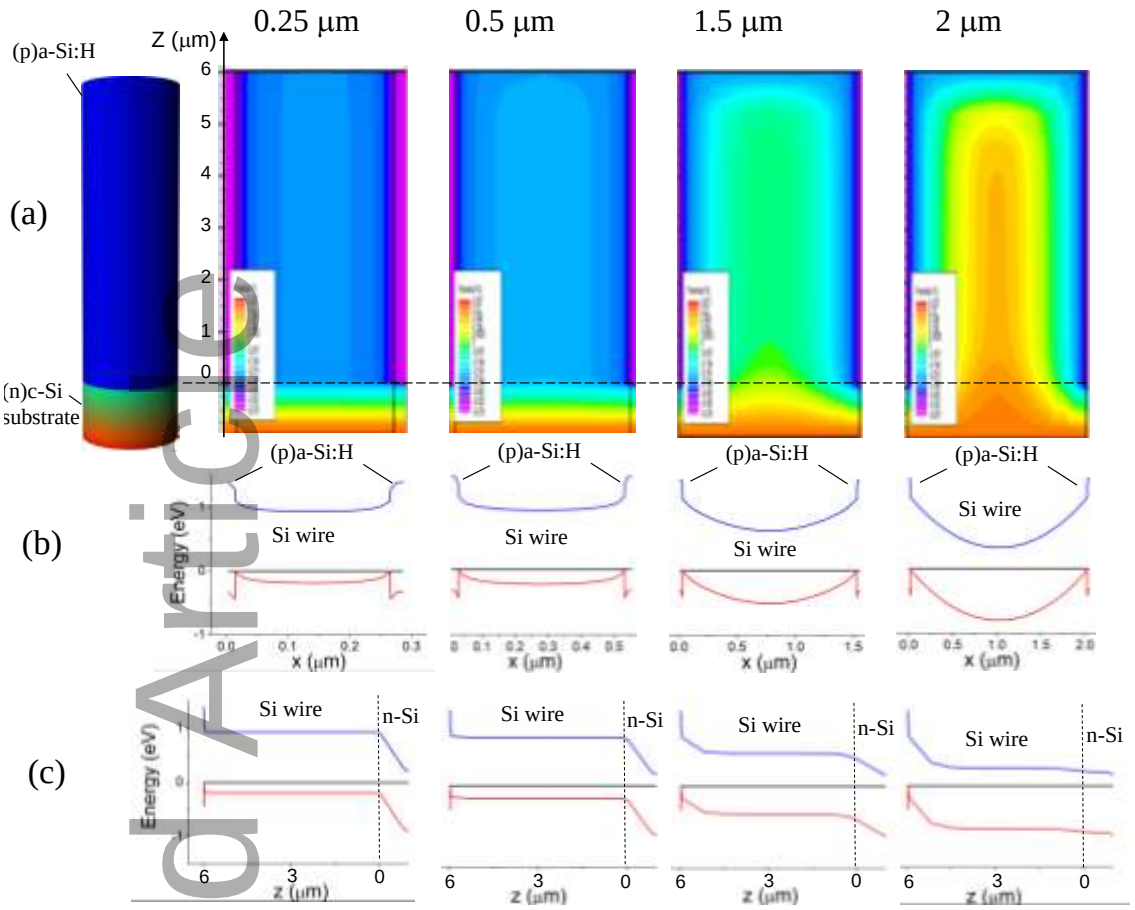

Figure 2. The potential profiles calculated for Si wires with a various diameter (0.25- 2 µm) (a). The calculated band diagrams across (b) and along (c) Si wires are also presented.

The absence of the required electric field at the a-Si:H/c-Si interface leads to the fact that excess charge carriers generated in the volume of n-Si wire can easily diffuse toward the surface. Thus, for nonnegligible density of interface states the interface recombination is strongly enhanced as demonstrated by the calculated EQE spectra presented in **Figure 3**. The presence of D_{it} (5×10^{11}–10^{12} $cm^{-2}eV^{-1}$) leads to a significant decrease in the quantum efficiency in the short-wavelength region compared to EQE calculated for zero density of states. Such behavior of fully inverted Si wires is completely different compared to that of planar a-Si:H/c-Si solar cells (Figure 1b). Moreover, in the case of Si wire inversion, the recombination losses rise with the wire height. The EQE spectra calculated for 0.25 and 0.5 µm Si wire structure with D_{it} of 10^{12} cm^{-2} eV^{-1} exhibit a drastic decrease of the short wavelength edge with increase of the height (**Figure 4**). Indeed, for higher height more

photons are absorbed in the inverted wire where the significant amount of generated charge carriers is recombined. The obtained decrease of the quantum efficiency with wire height is in good agreement with the experimental behavior observed in ref. [23].

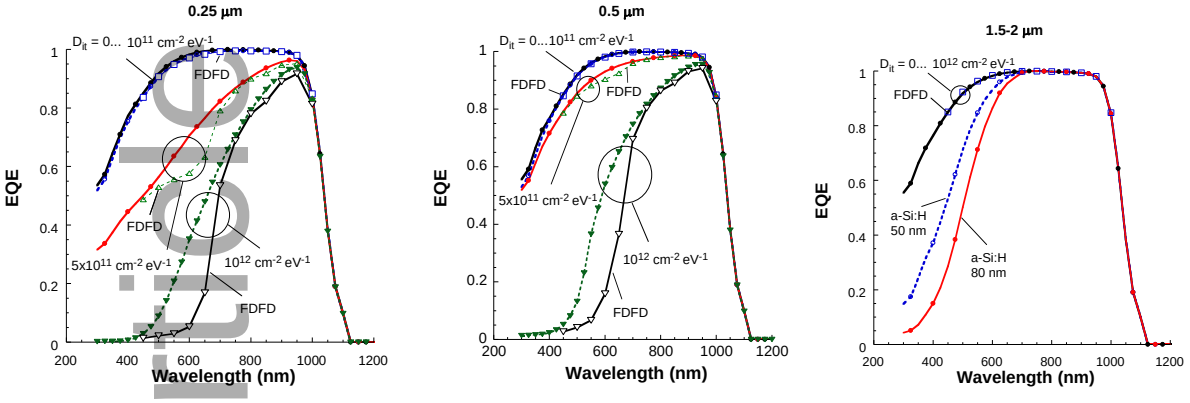

Figure 3. EQE spectra calculated using Beer–Lambert–Bouguer absorption and FDFD method for a-Si:H/c-Si heterojunction solar cells based on Si wires with diameter of 0.25 μm (a), 0.25 μm (b) and 1.5-2 μm (c) with D_{it} = 0 - 10^{12} cm^{-2} eV^{-1}. Spectra for diameter of 1.5 μm with D_{it} = 10^{12} cm^{-2} eV^{-1} and a-Si:H thickness of 50 and 80 nm are also presented (c).

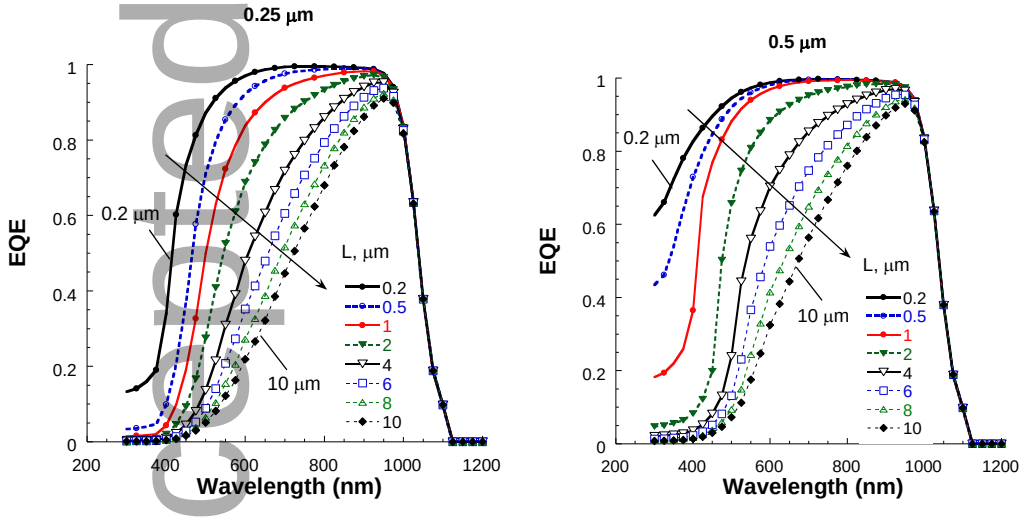

Figure 4. EQE spectra calculated for a-Si:H/c-Si heterojunction solar cells based on Si wires with diameter of 0.25 μm (a) and 0.5 μm (b) with D_{it} = 10^{12} cm^{-2} eV^{-1} for different wire height (L).

In case of the 1.5-2 μm Si wire, when its radius is comparable to the width of space charge region, a strong band bending at the (p)a-Si:H/(n)Si interface occurs. The band bending and therefore electric field prevents the diffusion of electrons and their recombination at the a-Si:H/c-Si interface. As a result, an increase in the interface states density does not affect the

quantum efficiency under the short circuit current conditions, as demonstrated by the simulation results presented in Figure 3.

A strong absorption enhancement could occur in nanowires due to self-concentration effect. [27] In order to study the influence of this effect on the quantum efficiency spectra the finite difference frequency domain (FDFD) simulations were performed with Comsol Multiphysics software. The calculation considered an elementary cell of a Si wire periodic structure, which contained one wire with variable diameter. The wire length was set equal to 2 μm with perfect matched layer on the bottom model boundary to study absorption of shortwave lights in the wires. Periodic boundary conditions were set at the cell boundaries to take into account the optical interaction between the wires. Calculation shows the Si wires absorb light much effectively compared to the bulk material due to self-concentration effect. The calculated enhancement of the absorption in the Si wire is demonstrated in **Figure 5**, where a ration of absorbed photons calculated by FDFD method to that calculated using Beer–Lambert–Bouguer absorption is presented**.** The absorption calculated by FDFD was used for the EQE spectra simulations (Figure 3). In principle, enhanced light absorption is an advantage of the Si wires for solar cell application. However, in case of small Si wire diameter (0.25-0.5 μm) with nonnegligible interface states (5×10^{11}–10^{12} $cm^{-2}eV^{-1}$), strong absorption in the wire leads to more pronounced decrease in EQE as demonstrated in Figure 3a,b, where the calculated spectra with FDFD absorption are presented. When the wires are fully inverted no electric field at the a-Si:H/c-Si radial interface leads to a strong recombination. The major part of the generated charge carriers recombines, and therefore enhanced absorption leads to enhanced recombination. In contrast, for wider Si wires (1.5-2 μm) increased absorption does not affect the EQE spectra (Figure 3c). As mentioned above the electric field at the a-Si:H/c-Si radial interface prevents the recombination under the short circuit conditions.

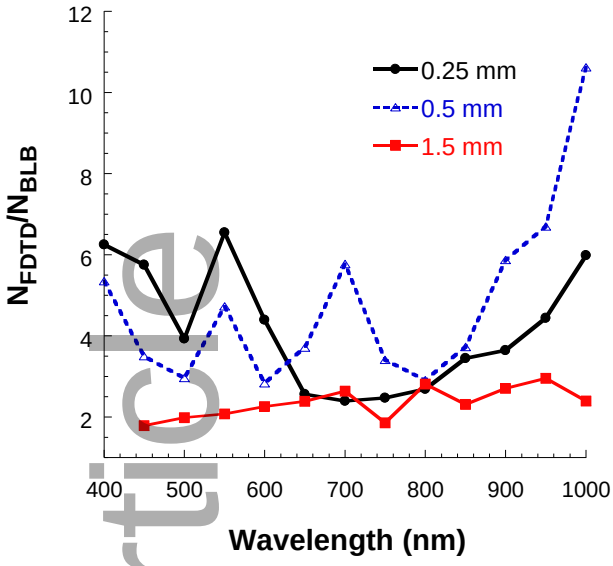

Figure 3. Ratio of absorbed photons calculated by FDFD method to that calculated by Beer–Lambert–Bouguer (BLB) law as a function on wavelength for Si wires with different diameter.

Thus, according to the calculations, the negative impact of the interface states on quantum efficiency may be avoided by using silicon wires whose radius exceeds the width of the space charge region. Taking into account that silicon with a doping level of 10^{15} - 10^{16} cm^{-3} is used for solar cells, the diameter of silicon wires should be more than 1 μm.

3. Experimental details

To confirm the revealed dependence of the sensitivity to surface states on the wire diameter, a comparative analysis of the calculation results with experimental data was carried out. FZ n-type Si substrates with a doping level of 2×10^{15} were used. Additional measurements were carried out using CZ Si substrates n-type doped to 10^{16} and 10^{17} cm^{-3}.

Si wires arrays with a height of 6 μm and diameter of 0.5 and 1.5 μm were fabricated using latex sphere lithography with an intermediate step of SiO_2 hard mask formation and cryogenic plasma etching.[28] Firstly, a 0.5 μm thick SiO_2 layer was deposited by PECVD on Si

substrates at 250 °C. The surface of SiO_2 was covered by latex spheres from a colloidal solution using spin coating. Latex spheres with diameters of 1 and 2 μm were used. Then, substrates were heated on a hot plate for 10 s at a temperature of 120 °C in order to avoid sphere migration during etching. Next, the substrates were loaded into a vacuum chamber of Oxford Instruments Plasmalab 100 ICP 380 setup and cooled down to -40 °C. Three subsequent dry etching steps were proceeded. First, the diameter of the spheres was reduced in oxygen plasma.[29] Secondly, SiO_2 was etched in CHF_3 plasma via latex spheres to form a hard mask. Inductively coupled plasma (ICP) with a power of 800 W accompanied by RF power of 30 W were applied. CHF_3 gas flow of 40 sccm and pressure of 5 mTorr were used to etch SiO_2.[30] Thirdly, deep cryogenic ICP etching of Si at a temperature of -140 °C was performed via the formed hard SiO_2 mask. The gas mixture of SF_6 (50 sccm) and O_2 (10 sccm) at pressure of 5 mTorr was used. The combination of ICP power of 1000 W and RF power of 30 W allows one to reach high aspect ratio (15:1) with etching rate about 1.3 μm /min.[28] Scanning electron microscopy (SEM) was used to control the etching process. An example of SEM image for 1.5 μm Si wire array is presented in **Figure 6**.

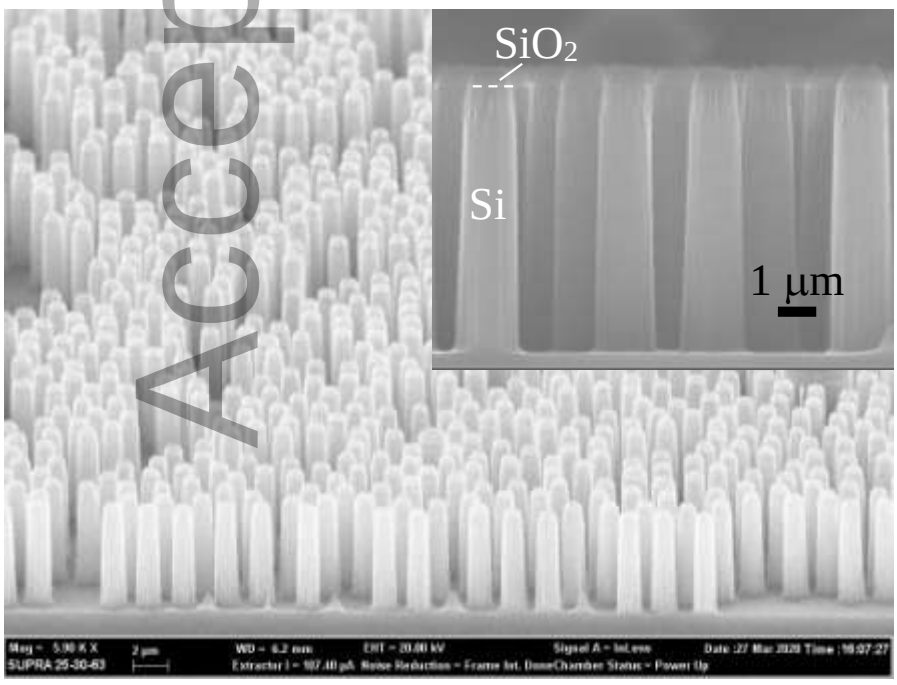

Figure 6. SEM image of 1.5 μm Si wire array obtained by dry etching. SiO_2 hard mask is not removed.

According to our previous study ICP cryogenic etching could damage the Si under-surface layer within a depth of about 30 nm, leading to a decrease of the effective charge carrier lifetime. Lifetime may be recovered by removing the damaged layer.[25] A special cleaning procedure was developed to prepare the samples before a-Si:H/c-Si heterojunction formation. The removal of residues of polystyrene spheres was carried out by boiling the samples sequentially in CCl_4, and then in isopropyl alcohol. After abundant water rinsing, the SiO_2 layer was removed in a 10 % HF/H_2O solution. After that, the damaged under-surface layer was removed in a 4% KOH solution at a temperature of 22 °C with simultaneous ultrasonic treatment for better removal of reaction products. Further cleaning was carried out according to the Shiraki method.[31]

To form a-Si:H/c-Si heterostructures based on of Si wires array, the layers of amorphous hydrogenated silicon (a-Si:H) were deposited by PECVD at a temperature of 250°C and a pressure of 350 mTorr using an Oxford PlasmaLab 100 setup. Contact a-Si:H layers were deposited in two steps. At the first step, a thin (3 nm) layer of undoped a-Si: H was deposited to passivate the Si surface. A pure silane (SiH_4) flow of 40 sccm and a minimum possible power density of 2.2 mW/cm^2 RF plasma (13.56 MHz) were used. Then the deposition of the doped layer was carried out. Immediately before loading into a vacuum chamber, the substrates were treated in a 10% HF/H_2O solution to remove the native oxide.

Firstly, 20 nm thick n-type phosphorus doped a-Si:H layer was deposited on the back side of Si substrates. A gas mixture of SiH_4 and 0.5% hydrogen diluted phosphine (PH_3/H_2) with flows of 40 sccm and 50 sccm, respectively, were used. At the next step, the front surface of the Si wires was covered by p-type a-Si:H layer. Due to the fact that the Si wires surface has a high aspect ratio, the deposition time of the undoped passivating and p-doped emitter layers was increased by factor of 3 compared to that of the planar structures. Immediately after the deposition of the passivation layer, a boron-doped a-Si:H layer was deposited. Gas flows of

SiH_4 and 2 % trimethylboron ($B(CH_3)_3/H_2$) diluted in hydrogen equal to 40 sccm and 50 sccm, respectively, were used. The resulting thicknesses of the passivating ((i)a-Si:H) and emitter ((p)a-Si:H) layers in terms of the planar surface were expected to be 10 nm and 60 nm, respectively. Transmission electron microscopy (TEM) and scanning electron microscopy (SEM) were used to study the structural properties of Si wires and control the a-Si:H deposition on the walls of the Si wires. TEM measurements were performed using Jeol JEM-2100F microscope (accelerating voltage 200 kV, point resolution 0.19 nm). Specimens for TEM were prepared by dry mechanical transfer of the wires onto a carbon lacey film supported by copper TEM-grid.

Finally, an ITO layer was sputtered on the front face of the a-Si:H/c-Si wire array to form the top electrode. Silver paste and vacuum evaporated Ag layer were used for the top and the bottom contacts, respectively. The complete solar cell structures were annealed at 180°C for 10 min to reduce contact resistance of the silver paste. Quantum efficiency spectra were measured using a Solar Laser M266 monochromator and a Stanford Research SRS850 lock-in amplifier. The I–V curves under AM1.5G simulator (Abet Technology SunLite) were measured using a Keithley 2400 sourcemeter.

4. Results and discussions

The TEM images of Si wire sidewall after wet chemical treatment are presented in **Figure 7**. The walls of Si wires have quite smooth surface (Figure 7a). No nano-porosity formation and other structural defects were observed at high resolution (Figure 7b). The Si wire surface is covered by native oxide of 2-3 nm thickness, which could be successfully removed by HF dip before a-Si:H deposition. The deposition of a-Si:H layers by PECVD at the vertical walls of the Si wires is a key issue for technology of solar cells fabrication. To control the covering of Si wires, TEM measurements were performed. The Si wire sidewalls are fully covered by a-Si:H as demonstrated by TEM (**Figure 8**) recorded from the different parts of the Si wire.

However, the thickness of a-Si:H layer at the vertical wall is lower compared to the planar surface and varies along the height. Thus, the total thickness of a-Si:H layers at the top of the Si wire is about 80-90 nm (Figure 8a), while at the upper part of the sidewall it is about 40-50 nm (Figure 8b), and at the down part it is reduced to 20-30 nm (Figure 8c). The variation of the thickness along the wires depends on the distance between them. This effect is demonstrated by SEM cross sections (**Figure 9**) for undoped 140 nm thick a-Si:H layer deposited on the Si substrates with slits etched using lithography and cryogenic ICP process. The slits are about 8 µm deep and have different widths. In case of 4 µm width slit, the thickness of a-Si:H reduced to 60-70 nm at the upper part of the sidewall and to 40-50 nm at the down part, remaining about 50 nm at the bottom (Figure 9a). However, for 1 µm width slit, the variation is much stronger. The thickness of a-Si:H layer is about 20 nm at the bottom and the down part of the sidewall (Figure 9b). This result obtained for the slits cannot be directly applied for estimation of the thickness of (i)a-Si:H layer at the Si wire sidewalls and the bottom due to different precursor limited conditions. However, on the one hand, we can conclude that all the surface of Si wires and the bottom is covered by a-Si:H preventing strong free surface recombination, but on the other hand, the thickness of the passivating (i)a-Si:H layer varies along the Si wires height. The last one is a serious issue because the optimal thickness of undoped a-Si:H being in the range 3-5 nm should be obtained for all surface of the a-Si:H/c-Si heterojunction. A higher thickness of (i)a-Si:H leads to drop in fill factor, while for lower thickness the recombination losses increase.

Thus, the further optimization of (i)a-Si:H layer deposition process should be carried out to increase the performance of a-Si:H/c-Si solar cells based on the Si wires.

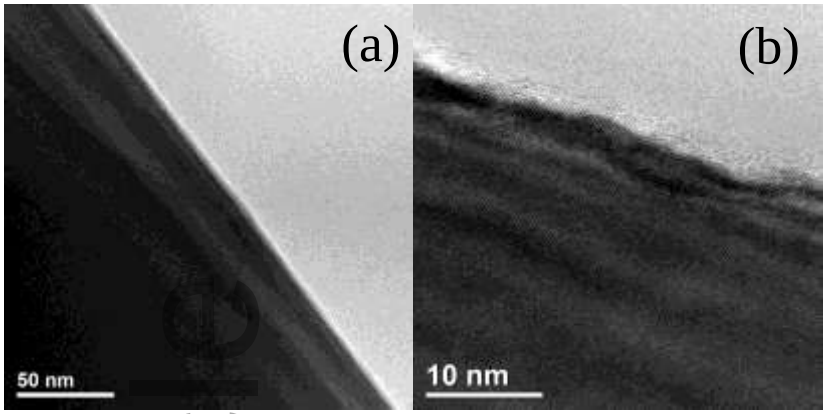

Figure 7. TEM images of the wall of Si wire after etching.

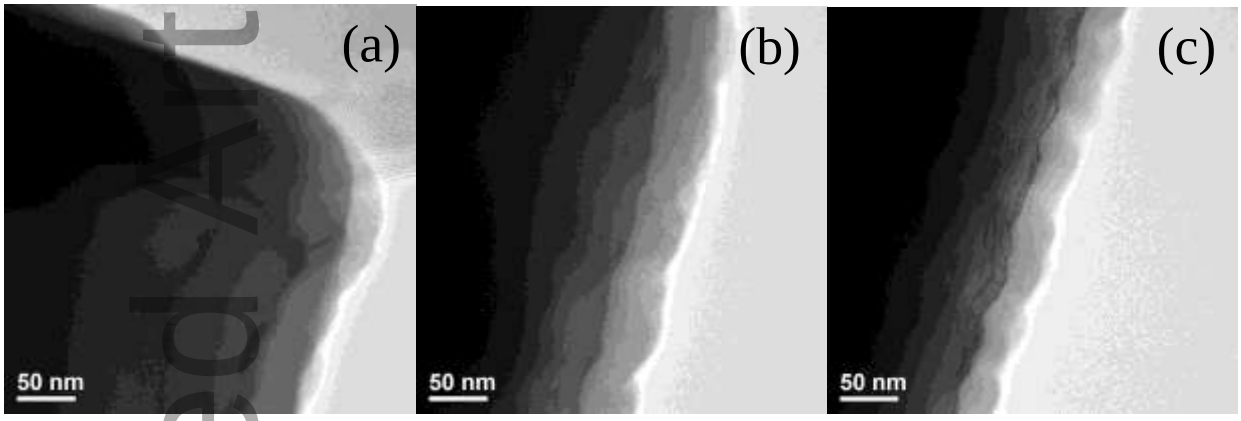

Figure 8. TEM images of the Si wire with a-Si:H layer deposited at the top (a), up (b) and down (c) parts of the sidewall.

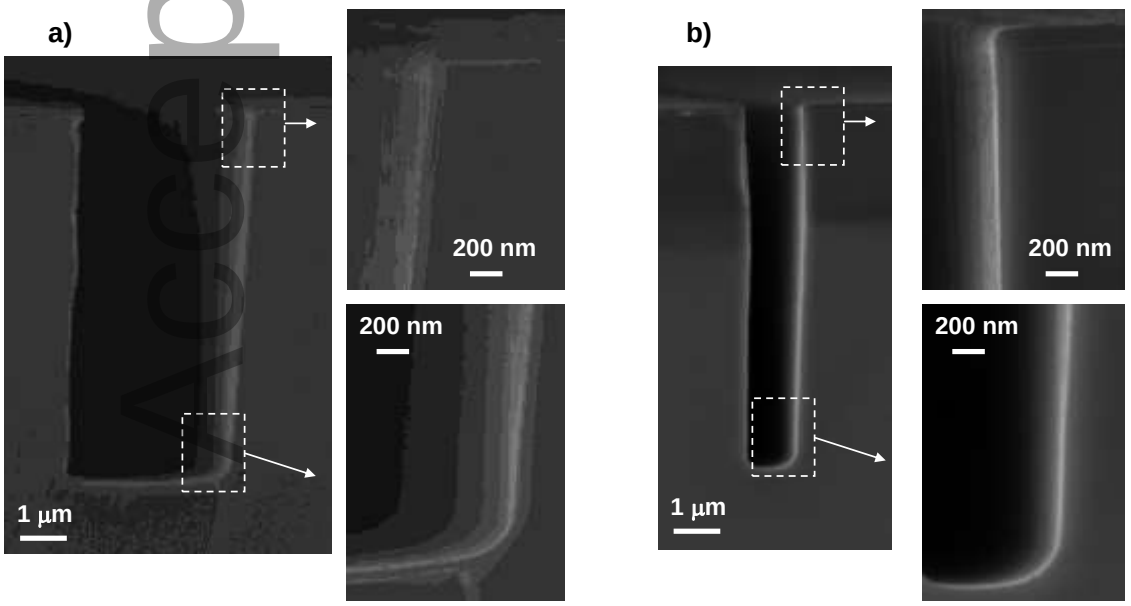

Figure 9. SEM images of the a-Si:H layer deposited on the Si substrates with etched gaps of 4 μm (a) and 1 μm width (b).

According to simulation (Figure 1a), as V_{oc} > 0.65 V can be achieved for planar (p)a-Si:H/(n)c-Si structures fabricated at the same deposition conditions, the value of D_{it} at the a-Si:H/c-Si interface is not expected to exceed 10^{12} cm^{-2} eV^{-1}. So, the similar D_{it} value at the Si wires sidewalls interface is expected.

Figure 10 presents *I-V* curves measured under AM1.5G illumination for a-Si:H/c-Si heterojunction solar cells based on Si wires of 0.5 μm and 1.5 μm in diameter. For each of the structures, V_{oc} equals to 0.5 V, which is much less than that for a planar heterojunction (0.65 V). For the Si wire structures, V_{oc} is obviously affected by enhanced contribution of recombination at the interface because its surface area is significantly higher.

However, it should be stressed that the same V_{oc} obtained for different structures indicates a similar defect density for them. In contrast, the values of the short circuit current for the structures are different, which should be analyzed using quantum efficiency spectra.

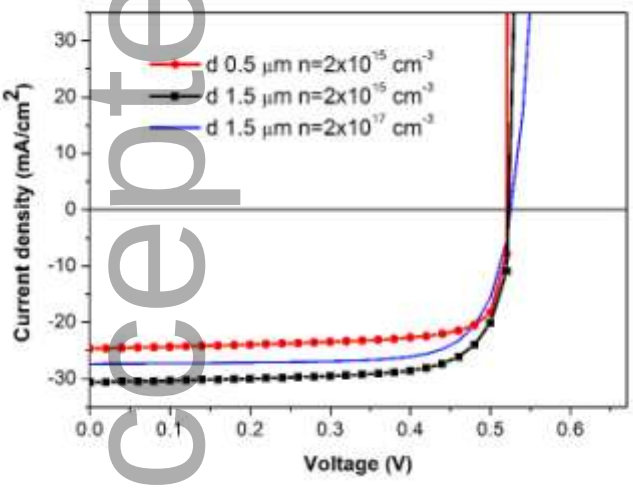

Figure 10. I-V curve under AM1.5G for structures with a-Si:H/Si heterojunction based on Si wires of 6 μm long with a diameter of 0.5 μm (2×10^{15} cm^{-3}) and 1.5 μm (2×10^{15} cm^{-3} and 10^{17} cm^{-3}).

The external quantum efficiency (EQE) spectra are presented in **Figure 11**. It should be noted that high a-Si:H total thickness (50-80 nm) leads to stronger optical losses in short wave region for all the structures as demonstrated by simulations (Figure 3c). However, EQE

spectra show a significant difference between the structures based on silicon wires with a diameter of 0.5 μm and 1.5 μm. The quantum efficiency of 0.5 μm Si wire diameter structures is significantly lower compared to that of 1.5 μm wire structures. The drop in EQE for structures with a smaller diameter is more pronounced in the short-wavelength region, which is in full agreement with the simulation results. At a doping level of 2×10^{15} cm^{-3}, the width of the space charge region is approximately 0.6 μm. The wires with a diameter of 0.5 μm are completely depleted, and therefore, the electric field at the a-Si:H/Si interface is absent along the entire lateral surface of the wires, which leads to increased recombination at the interface states. When the wire diameter is 1.5 μm, the band bending, and hence the electric field, extends along all the side surfaces of the silicon wires. In this case, the sensitivity to interface states is much lower. For a-Si:H/Si heterostructures with a diameter of 1.5 μm fabricated using silicon with a doping level of 10^{17} cm^{-3}, the short-wavelength EQE edge is almost identical to the spectra of the structures formed on Si wires doped with 2×10^{15} cm^{-3}. Taking into account that, for highly doped silicon, the band bending at the a-Si:H/Si interface is stronger, the identity of the EQE spectra in the short-wavelength region indicates that they are not affected by interface states for both structures with a diameter of 1.5 μm. The differences in the long-wavelength region of the spectra are due to the shorter volume lifetime of charge carriers in heavily doped silicon, which is associated with the prevailing Auger recombination. Since the structures are formed on Si substrates with a thickness of about 300 μm, significant differences in the bulk lifetime (10 ms for 2×10^{15} cm^{-3} and 50 μs for 10^{17} cm^{-3}) lead to a difference in EQE in the long-wavelength region due to recombination in the bulk of the substrate.

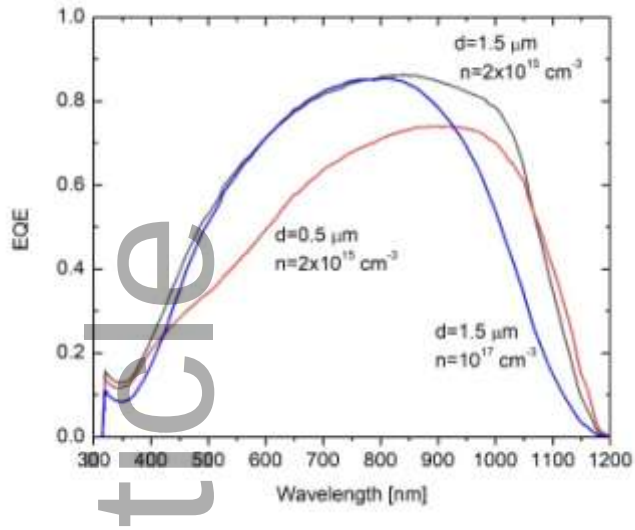

Figure 11. Experimental spectra of external quantum efficiency for structures with a-Si:H/Si heterojunction based on Si wires of 6 μm long with a diameter of 0.5 μm (2×10^{15} cm^{-3}) and 1.5 μm (2×10^{15} cm^{-3} and 10^{17} cm^{-3}).

The structures with different Si wire diameter and doping level represent three cases: fully inverted Si wire (0.5 μm, 2×10^{15} cm^{-3}), slightly (1.5 μm, 2×10^{15} cm^{-3}) and extremely (1.5 μm, 10^{17} cm^{-3}) above the depletion limit. The fact that the structures with different levels of Si wires depletion demonstrate the same value of V_{oc}, while have strong difference for EQE, is in agreement with simulation results and can be explained in terms of band diagrams. For open circuit conditions, the bands at the a-Si:H/Si interface are flat due to external voltage and therefore, band bending does not depend of Si wire size. The value of V_{oc} is determined by D_{it}, which is expected to be at the same level for all the structures. In contrast, for short circuit current conditions the band bending and therefore sensitivity to D_{it} depends on Si wire diameter. Similar effect was also experimentally demonstrated for Si wire core-shell p-n junction fabricated by phosphorus diffusion. [32] Drop of the quantum efficiency with decrease of the Si diameter was observed for low doping level, while V_{oc} was not affected. The same recommendation to scaling the microwire diameter with the depletion width was suggested. Thus, the band bending should be taken into account when designing solar cells based on Si wires. However, we should stress that fully inverted Si wires have one unexpected advantage.

Indeed, the conductivity of the inverted Si wire drastically increases providing better spreading of the emitter layer that leads to higher fill factor of *I-V* curves. This effect opens a new way for further improvement of solar cell performance if low a-Si:H/c-Si radial interface density reached.

5. Conclusion

The influence of Si wire diameter on the sensitivity to the interface states of a-Si:H/c-Si core-shell solar cells was demonstrated using simulation and experimental measurements. A decrease of Si wire diameter leads to wire inversion and an increase of the sensitivity to interface states on the sidewall for the short-circuit condition. When the Si wire is completely inverted, a lack of band bending at the a-Si:H/c-Si interface leads to a sharp increase of the recombination level. For open circuit conditions, the effect of complete inversion of Si wires does not affect the sensitivity to interface states, since the bands are already flat.

Thus, for structures based on Si wires with a radius smaller than the space-charge region, losses related to interface recombination increase, and a decrease of the quantum efficiency in the short-wavelength region is observed. To reduce recombination losses, it is necessary to use silicon wires with a radius exceeding the space charge region in silicon.

Acknowledgements

This work was supported by the Ministry of Science and Higher Education of the Russian Federation (research project 0791-2020-0004). TEM studies were performed using equipment of the Federal Joint Research Center “Material science and characterization in advanced technology” supported by the Ministry of Science and Higher Education of the Russian Federation (id RFMEFI62119X0021).

Received: ((will be filled in by the editorial staff))
Revised: ((will be filled in by the editorial staff))
Published online: ((will be filled in by the editorial staff))

References

[1] M. Bivour, M. Reusch, S. Schröer, F. Feldmann, J. Temmler, H. Steinkemper, M. Hermle, *IEEE Journal of Photovoltaics.* **2014**, *4*, 566.

[2] K. Yoshikawa, H. Kawasaki, W. Yoshida, T. Irie, K. Konishi, K. Nakano, T. Uto, D. Adachi, M. Kanematsu, H. Uzu, K. Yamamoto, *Nature Energy.* **2017**, *2*, 17032.

[3] D. Adachi, J. L. Hernandez, K. Yamamoto, *Appl. Phys. Lett*. **2015**, *107*, 233506.

[4] K. Masuko, M. Shigematsu, T. Hashiguchi, D. Fujishima, M. Kai, N. Yoshimura, T. Yamaguchi, Y. Ichihashi, T. Yamanishi, T. Takahama, M. Taguchi, E. Maruyama, S. Okamoto, *IEEE Journal of Photovoltaics.* **2014**, *4(6)*, 1433.

[5] V. Sivakov, F. Voigt, B. Hoffmann, V. Gerliz, S. Christiansen, in *Nanowires* (Ed: A. Hashim), Intech, London, UK **2011**, Ch. 3.

[6] A. I. Hochbaum, R. Fan, R. He, P. Yang, *Nano Letters.* **2005**, *5*, 457.

[7] B. A. Buchine, F. Modawar, M. R. Black (Bandgap Engineering Inc.) *US8143143B2*, **2012**.

[8] V. Sivakov, G. Andrä, A. Gawlik, A. Berger, J. Plentz, F. Falk, S. H. Christiansen, *Nano Letters.* **2009,** 9, 1549.

[9] B. M. Kayes, N. S. Lewis, H. A. Atwater, *J. Appl. Phys*. **2005**, *97*, 114302.

[10] V. Sivakov, F. Voigt, G. Bauer, S. H. Christiansen, *Phys. Rev.* **2010**, *82*, 125446.

[11] L. Tsakalakos, J. Balch, J. Fronheiser, A. Korevaar, O. Sulima, J. Rand, *Appl. Phys. Lett*. **2007**, *91*, 233117.

[12] M. D. Kelzenberg, D. B. Turner-Evans, B. M. Kayes, M. A. Filler, M. C. Putnam, N. S. Lewis, H. A. Atwater, *Nano Letters.* **2008**, *8*, 710.

[13] M. C. Putnam, S. W. Boettcher, M. D. Kelzenberg, D. B.Turner-Evans, J. M. Spurgeon, E. L. Warren, R. M. Briggs, N. S. Lewis, H. A. Atwater, *Energy Environ. Sci.* **2010**, *3*, 1037.

[14] E. C. Garnett and P. Yang, *J. Am. Chem. Soc*. **2008**, *130*, 9224.

[15] A. Dalmau Mallorquí, E. Alarcón-Lladó, I. Canales Mundet, A. Kiani, B. Demaurex, S. De Wolf, A. Menzel, M. Zacharias, A. Fontcuberta i Morral, *Nano Research* **2015**, 8, 673

[16] M.-V. Fernandez-Serra, Ch. Adessi, and X. Blasé, *Nano Lett.* **2006**, 6, 2674.

[17] Sh.Yu, F. Roemer, B. Witzigmann, *Journal of Photonics for Energy.* **2012**, 2, 028002

[18] T. Mueller, S. Schwertheim, W.R. Fahrner, *J. Appl. Phys.* **2010**, *107*, 014504.

[19] N. Jensen, U. Rau, R.M. Hausner, S. Uppal, L. Oberbeck, R.B. Bergmann, J.H. Werner, *J. Appl. Phys.* **2000**, *87*, 2639.

[20] A. Froitzheim, K. Brendel, L. Elstner, W. Fuhs, M. Schmidt, *J. Non-Cryst. Solids.* **2002**, *299-302*, 663.

[21] M. Schmidt, L. Korte, A. Laades, R. Stangl, Ch. Schubert, H. Angermann, E. Conrad, *Thin Solid Films.* 2007, *515*, 7475.

[22] Y. Dan, K. Seo, K. Takei, J. H. Meza, A. Javey, K. B. Crozier, *Nano Lett.* **2011**, 11, 2527.

[23] I. A. Morozov, A. S. Gudovskikh, D. A. Kudryashov, E. V. Nikitina, F. Talkenberg, A. Schleusener, A. Bochmann, V. Sivakov, *J. Nanoelectr. and Optoelectr.* **2014**, *9(6)*, 723.

[24] R.Stangl, C.Leendertz, J.Haschke. in *Solar Energy*, InTech, **2010** (doi:10.5772/8073)

[25] D. A. Kudryashov, A. S. Gudovskikh, A. I. Baranov, I. A. Morozov, A. O. Monastyrenko, *Phys. Status Solidi A.* **2020**, *217*, 1900534.

[26] J.-P. Kleider, J. Alvarez, A.V. Ankudinov, A.S. Gudovskikh,E.V. Gushchina,M. Labrune, O.A. Maslova, W. Favre,M.-E. Gueunier-Farret, P. Rocai Cabarrocas, E.I. Terukov, *Nanoscale Res Lett.* **2011**, 6, 152.

[27] M. Heiss, E. Russo-Averchi, A. Dalmau-Mallorqu, G. Tutuncuoglu, F. Matteini, D. Ruffer, S. Conesa-Boj, O. Demichel, E. Alarcon-Llado, A. Fontcuberta i Morral, *Nanotechnology* **2014** 25, 014015.

[28] I. Morozov, A. Gudovskikh, A. Uvarov, A. Baranov, V. Sivakov, D. Kudryashov, *Phys. Status Solidi A.* **2020**, *217*, 1900535.

[29] I. A. Morozov, K. A. Vyacheslavova, A. S. Gudovskikh, A. V. Uvarov, A. I. Baranov, D. A. Kudryashov, *J. Phys. Conf. Ser.* **2020,** *1697*, 012192.

[30] E. A. Vyacheslavova, I. A. Morozov, D. A. Kudryashov, A. S. Gudovskikh, *J. Phys. Conf. Ser.* **2020**, *1697*, 012188.

[31] A. Ishizaka, Y. Shiraki, *J. Electrochem. Soc.* **1986**, *133*, 666.

[32] A. Dalmau Mallorquı, F. M. Epple, D. Fan, O. Demichel, A. Fontcuberta i Morral, *Phys. Status Solidi A.* **2012**, 209, 1588.

The impact of interface states on the quantum effciency of a-Si:H/c-Si solar cells based on Si wires is studied using simulation and experimental measurements. The key role of the Si wire geometry for sensitivity of quantum efficiency to interface states on the sidewall is demonstrated.